Electronic Absorption Spectroscopy of Cobalt Ions in Diluted Magnetic Semiconductor Quantum Dots: Demonstration of an Isocrystalline Core/Shell Synthetic Method

Pavle V. Radovanovic and Daniel R. Gamelin*

Contribution from the Department of Chemistry, Box 351700, University of Washington, Seattle, Washington 98195-1700

Received June 22, 2001

Abstract: This paper reports the application of ligand-field electronic absorption spectroscopy to probe Co^{2+} dopant ions in diluted magnetic semiconductor quantum dots. It is found that standard inverted micelle coprecipitation methods for preparing Co^{2+}-doped CdS (Co^{2+}:CdS) quantum dots yield dopant ions predominantly bound to the nanocrystal surfaces. These Co^{2+}:CdS nanocrystals are unstable with respect to solvation of surface-bound Co^{2+}, and time-dependent absorption measurements allow identification of two transient surface-bound intermediates involving solvent−cobalt coordination. Comparison with Co^{2+}:ZnS quantum dots prepared by the same methods, which show nearly isotropic dopant distribution, indicates that the large mismatch between the ionic radii of Co^{2+} (0.74 Å) and Cd^{2+} (0.97 Å) is responsible for exclusion of Co^{2+} ions during CdS nanocrystal growth. An isocrystalline core/shell preparative method is developed that allows synthesis of internally doped Co^{2+}:CdS quantum dots through encapsulation of surface-bound ions beneath additional layers of CdS.

I. Introduction

Semiconductor quantum dots (QDs) have emerged as an attractive class of materials for photonics applications.[1−3] Recently, attention has turned to the unusual optical, magnetic, and photophysical phenomena observed when QDs are doped with paramagnetic impurities to form diluted magnetic semiconductor QDs (DMS-QDs).[4−14] Among bulk DMS materials, Mn^{2+}-doped II−VI semiconductors have received extraordinary attention due to their giant Faraday rotation and magnetoresistance effects, both of which arise from strong sp−d exchange interactions between the semiconductor band electrons and the unpaired spin density localized on the dopant ion.[15] Additionally, Mn^{2+} is an efficient luminescence activator in these materials.[16] There is growing evidence that some of these properties may be enhanced by quantum confinement in high-quality DMS-QDs.[5,7,11,17]

A major obstacle in the preparation of high-quality DMS-QDs is the rapid increase in surface-to-volume ratios as particle diameters are reduced to strong quantum confinement dimensions (e.g $<\sim$5.2 nm in CdS[18]). Surface-bound impurity ions are subject to low-symmetry distortions, solvent interactions, and potentially poor coupling with the semiconductor band electrons. Consequently, the desired physical properties of DMS-QDs may be compromised if dopants are not properly incorporated within the QD lattice. Simple coprecipitation of Mn^{2+}-doped CdS (Mn^{2+}:CdS) and CdSe (Mn^{2+}:CdSe) QDs has been found to yield predominantly surface-bound impurities,[4,19] however, indicating that extreme care must be taken to ensure and demonstrate internal doping when preparing such samples. The use of organometallic Mn^{2+} precursors instead of simple Mn^{2+} salts has been shown to improve internal doping of Mn^{2+} into CdSe QDs made by coprecipitation.[4] These synthetic challenges are compounded by difficulties in reliably distinguishing between surface-bound and internally doped impurity ions. EPR,[4−10] emission,[5−13] and EXAFS[14] spectroscopies, as

* Corresponding author. E-mail: Gamelin@chem.washington.edu.

(1) Special Issue on Semiconductor Quantum Dots. *MRS Bull.* **1998**, *23*, No. 2.

(2) Special Issue on Nanoscale Materials. *Acc. Chem. Res.* **1999**, *32*, No. 5.

(3) Klimov, V. I.; Mikhailovsky, A. A.; Xu, S.; Malko, A.; Hollingsworth, J. A.; Leatherdale, C. A.; Eisler, H.-J.; Bawendi, M. G. *Science* **2000**, *290*, 314−317.

(4) Mikulec, F. V.; Kuno, M.; Bennati, M.; Hall, D. A.; Griffin, R. G.; Bawendi, M. G. *J. Am. Chem. Soc.* **2000**, *122*, 2532−2540.

(5) Norris, D. J.; Yao, N.; Charnock, F. T.; Kennedy, T. A. *Nano Lett.* **2001**, *1*, 3−7.

(6) Bhargava, R. N. *J. Lumin.* **1996**, *70*, 85−94.

(7) Hoffman, D. M.; Meyer, B. K.; Ekimov, A. I.; Merkulov, I. A.; Efros, A. L.; Rosen, M.; Counio, G.; Gacoin, T.; Boilot, J.-P. *Solid State Commun.* **2000**, *114*, 547−550.

(8) Counio, G.; Esnouf, S.; Gacoin, T.; Boilot, J.-P. *J. Phys. Chem.* **1996**, *100*, 20021−20026.

(9) Feltin, N.; Levy, L.; Ingert, D.; Pileni, M.-P. *J. Phys. Chem. B* **1999**, *103*, 4−10.

(10) Chen, W.; Sammynaiken, R.; Huang, Y.; Malm, J.-O.; Wallenberg, R.; Bovin, J.-O.; Zwiller, V.; Kotov, N. A. *J. Appl. Phys.* **2001**, *89*, 1120−1129.

(11) Bhargava, R. N.; Gallagher, D.; Hong, X.; Nurmikko, A. *Phys. Rev. Lett.* **1994**, *72*, 416−420.

(12) Tanaka, M.; Qi, J.; Masumoto, Y. *J. Lumin.* **2000**, *87−89*, 472−474.

(13) Bol, A. A.; Meijerink, A. *Phys. Rev. B* **1998**, *58*, 15997−16000.

(14) Soo, Y. L.; Ming, Z. H.; Huang, S. W.; Kao, Y. H.; Bhargava, R. N.; Gallagher, D. *Phys. Rev. B* **1994**, *50*, 7602−7607.

(15) Diluted Magnetic Semiconductors; Furdyna, J. K., Kossut, J., Eds. In *Semiconductors and Semimetals*; Willardson, R. K., Beer, A. C., Eds.; Academic Press: New York, 1988; Vol. 25.

(16) Langer, D.; Ibuki, S. *Phys. Rev.* **1965**, *138*, A809−A815 and references therein.

(17) Oka, Y.; Yanata, K. *J. Lumin.* **1996**, *70*, 35−47.

(18) Vossmeyer, T.; Katsikas, L.; Giersig, M.; Popovic, I. G.; Diesner, K.; Chemseddine, A.; Eychmüller, A.; Weller, H. *J. Phys. Chem.* **1994**, *98*, 7665−7673.

(19) Ladizhansky, V.; Hodes, G.; Vega, S. *J. Phys. Chem. B* **1998**, *102*, 8505−8509.

10.1021/ja0115215 CCC: $20.00
Published on Web 11/16/2001

well as magnetic susceptibility,[9] have been employed as direct probes of dopant ions within DMS-QDs, and ^{113}Cd NMR has been successfully employed as an indirect probe of paramagnetic dopant ions in CdS and CdSe QDs.[4,19,20]

The sp−d exchange interactions in bulk Co^{2+}-doped II−VI semiconductors have been shown to be significantly larger than those in the analogous Mn^{2+}-doped DMS materials.[21,22] The possibility that novel magnetooptical phenomena may arise from quantum confinement in these DMS materials has motivated our synthesis and characterization of Co^{2+}-doped II−VI DMS-QDs. Previous studies of Co^{2+}-doped II−VI nanocrystals have used only ^{113}Cd NMR[20] and semiconductor band gap emission[23] to probe doping. ^{113}Cd NMR spectra of Co^{2+}:CdS QDs prepared by aqueous coprecipitation showed transferred hyperfine interactions between Co^{2+} and Cd^{2+} ions indicating that at least some of the Co^{2+} ions were incorporated substitutionally in the particles.[20] Co^{2+}:ZnS QDs prepared by a similar method showed apparent sensitization of band gap emission at low doping levels (<1.5%), but the location of the Co^{2+} ions in these ZnS QDs was not addressed.[23]

In this study we use ligand-field electronic absorption spectroscopy as a direct and sensitive probe of Co^{2+} dopant ions in Co^{2+}:CdS and Co^{2+}:ZnS DMS-QDs. The ligand-field electronic absorption properties of dopant ions in DMS-QDs have not received any previous attention, undoubtedly in part because of the low doping concentrations used (typically 1−10 dopant ions per QD), and in part because of the general literature focus on Mn^{2+}, which has exceptionally small absorption oscillator strengths.[24] We show here that this technique allows conclusive distinction between internally doped and surface-bound Co^{2+} ions in these DMS-QD materials. Using standard literature inverted micelle coprecipitation methods, we find that Co^{2+} ions bind almost exclusively to the surfaces of CdS nanocrystals, and are slowly solvated in the presence of coordinating solvents. In contrast, Co^{2+}:ZnS QDs synthesized by the same method show Co^{2+} ligand-field absorption spectra similar to those of bulk Co^{2+}:ZnS, indicating internal doping of the ZnS nanocrystalline lattice. These Co^{2+}:ZnS QDs are stable in the presence of coordinating solvents. The difference between CdS and ZnS nanocrystal doping is attributed to a large mismatch between dopant and host cationic radii in the case of CdS. Using this information, we have developed an isocrystalline core/shell synthetic methodology that yields stable, internally doped Co^{2+}:CdS QDs with Co^{2+} transition energies closely resembling those of bulk Co^{2+}:CdS. In cases where dopant/host incompatibilities occur, this isocrystalline core/shell method thus provides a simple and effective route to obtaining high-quality internally doped DMS-QDs.

II. Experimental Section

A. Sample Preparation. (i) Standard Synthesis of Co^{2+}-Doped CdS and ZnS QDs. The following procedure is based on literature methods,[8,9,26,27] and for convenience is referred to as the "standard" method, against which others may be compared. Two inverted micelle solutions were prepared from *n*-heptane/AOT/water ternary mixtures (AOT = dioctyl sulfosuccinate, sodium salt), one containing Na_2S and the other a mixture of $Cd(NO_3)_2$ (or $Zn(NO_3)_2$) and $Co(NO_3)_2$. Both solutions were made by dissolving the same amounts of AOT in identical volumes of heptane (6.25 g of AOT and 21.2 mL of heptane) and adding 1 mL of the appropriate aqueous stock solutions (0.38 M Na_2S,and 0.2 M $Cd(NO_3)_2$ or $Zn(NO_3)_2$ with 0.002−0.004 M $Co(NO_3)_2$). The inverted micelle solutions were briefly evacuated, degassed by bubbling with N_2, and mixed in the N_2 atmosphere. The resulting particles were capped and precipitated with pyridine under air-free conditions, and the solvent was evacuated on a Schlenk line. The precipitate was washed multiple times with petroleum ether and ethanol, dried under vacuum, and dispersed in pyridine to give a clear, completely transparent sol solution. Particles capped with dodecanethiol were prepared in an analogous fashion: after coprecipitation in inverted micelles, a small amount of dodecanethiol (∼100 μL) was added, and the solvent evacuated. The precipitate was washed with ethanol, vacuum dried, and dispersed in heptane. Samples made with intentional loading of the nanocrystal surfaces with Co^{2+} were prepared in an analogous fashion to that described above, with the exception that no Co^{2+} was included in the initial aqueous solutions. $Co(NO_3)_2$ was added after CdS particle formation, prior to capping with pyridine, and the particles were washed and suspended in pyridine as described above.

(ii) Isocrystalline Core/Shell Synthesis of Co^{2+}-Doped CdS and ZnS QDs. This procedure begins with the synthesis of the doped particles as described above. After particle formation but prior to capping, 1 mL of 0.2 M $Cd(NO_3)_2$ or $Zn(NO_3)_2$ and 1 mL of 0.2 M Na_2S were alternately added dropwise in the air-free environment over a period of ca. 20 min. The particles were then capped and precipitated with pyridine, and the remainder of the procedure described above was completed.

B. Data Collection and Analysis. Electronic absorption spectra were collected at room temperature with a Cary 5E (Varian) spectrophotometer and quartz cuvettes 1.0 cm in length. For Co^{2+}:CdS and Co^{2+}:ZnS DMS-QD ligand-field absorption experiments, solutions were ca. 1.5×10^{-3} M in Co^{2+}, while for Co^{2+}:CdS DMS-QD band gap absorption, samples were ca. 1.1×10^{-6} M in Co^{2+}. Because of pyridine interference, band gap absorption spectra for Co^{2+}:ZnS QDs were collected on thin-film samples deposited on quartz disks by solvent evaporation. Average particle sizes were estimated from literature relationships between band gap absorption energies and particle diameters.[18,28−30] Since band gap energies are sensitive to changes in the surrounding dielectric medium, these particle diameters should be considered approximate in absolute terms. Co^{2+} doping concentrations were determined by inductively coupled plasma atomic emission spectrometry (ICP-AES, Jarrel Ash model 955). Ligand-field calculations within the framework of the Angular Overlap Model (AOM) were performed with Ligfield, v. 0.92 (J. Bendix, Department of Chemistry, University of Copenhagen, 1998). For the 15 K electronic absorption spectra provided in the Supporting Information, samples were cooled by helium vapor by using a Janis STVP-100 continuous flow optical cryostat mounted in the absorption spectrophotometer.

III. Results

Figure 1a presents the absorption spectrum of 2.3% Co^{2+}:CdS QDs (in pyridine) synthesized by the standard inverted micelle coprecipitation method (see Section II.A.i). The left panel shows the CdS QD band gap absorption feature, from which the average particle diameter was estimated to be 3.0

(20) Ladizhansky, V.; Vega, S. *J. Phys. Chem. B* **2000**, *104*, 5237−5241.
(21) Zielinski, M.; Rigaux, C.; Lemaître, A.; Mycielski, A.; Deportes, J. *Phys. Rev. B* **1996**, *53*, 674−685.
(22) Seong, M. J.; Alawadhi, H.; Miotkowski, I.; Ramdas, A. K.; Miotkowska, S. *Phys. Rev. B* **2001**, *63*, 125208−(1−7).
(23) Yang, P.; Lü, M.; Xü, D.; Yuan, D.; Song, C.; Zhou, G. *J. Phys. Chem. Solids* **2001**, *62*, 1181−1184.
(24) Examples of ligand-field luminescence excitation spectra in DMS-QDs have been reported (for Mn^{2+} ions),[10,12,25] but these experiments are limited to dopant ions that are emissive, excluding many nonluminescent ions that may have interesting magnetooptical properties. Furthermore, luminescence excitation intensities may be strongly influenced by nonradiative effects and experimental parameters, and are therefore not readily analyzed quantitatively. Ligand-field absorption spectroscopy thus represents a valuable complementary experimental technique.
(25) Chen, W.; Sammynaiken, R.; Huang, Y. *J. Appl. Phys.* **2000**, *88*, 5188−5193.
(26) Levy, L.; Ingert, D.; Feltin, N.; Pileni, M.-P. *Adv. Mater.* **1998**, *10*, 53−57.
(27) Levy, L.; Feltin, N.; Ingert, D.; Pileni, M.-P. *Langmuir* **1999**, *15*, 3386−3389.
(28) Suyver, J. F.; Wuister, S. F.; Kelly, J. J.; Meijerink, A. *Nano Lett.* **2001**, *1*, 429−433.
(29) Brus, L. E. *J. Phys. Chem.* **1986**, *90*, 2555−2560.
(30) Lippens, P. E.; Lannoo, M. *Phys. Rev. B* **1989**, *39*, 10935−10942.

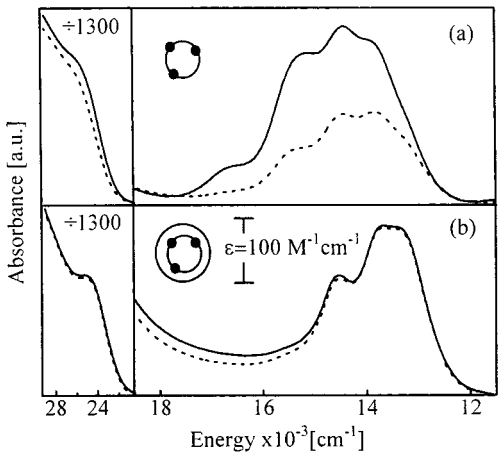

Figure 1. (a) Absorption spectra (300 K) of 3.0 nm diameter 2.3% Co^{2+}:CdS QDs in pyridine colloid solution, showing the CdS band gap transitions (left panels) and the Co^{2+} ν_3 ligand-field transitions (right panels). Note the different *x*- and *y*-axes for the two energy regions. The solid line was collected 2 h and the dashed line 23 h after synthesis. The inset illustrates solvation of Co^{2+} over time when no shell is present. (b) Absorption spectra (300 K) of 3.7 nm diameter 0.9% Co^{2+}:CdS QDs prepared by the isocrystalline core/shell method 2 (solid line) and 28 h (dashed line) after synthesis.

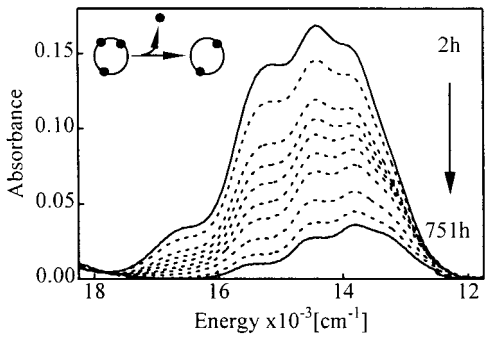

Figure 2. Ligand-field absorption spectrum (300 K) of the Co^{2+}:CdS QD sample from Figure 1a in pyridine colloid solution collected at several times after synthesis. Absorption decreases and shifts to lower energy with time. Times after synthesis (with decreasing absorption intensity): 2, 2.83, 4.25, 6, 10, 23, 46, 85, 199, and 751 h.

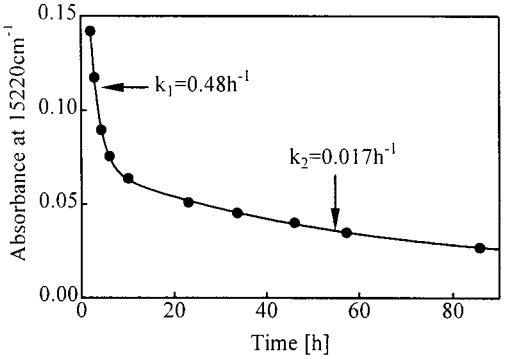

Figure 3. Decay of Co^{2+}:CdS QD ligand field absorption intensity from Figure 2 monitored at 15220 cm^{-1}. The solid line shows a biexponential best fit, yielding the rate constants indicated.

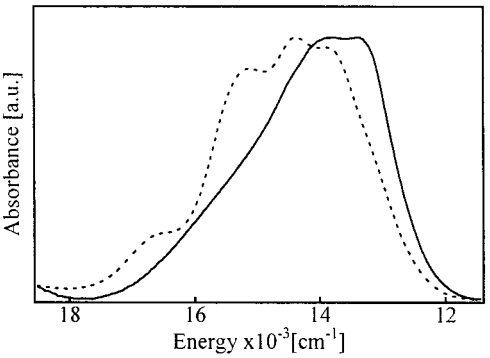

Figure 4. Normalized 300 K ligand field absorption spectra of 3.0 nm diameter 1.0% Co^{2+}:CdS QDs capped with dodecanethiol and suspended in heptane (solid line) and 3.2 nm diameter 7.5% Co^{2+}:CdS QDs prepared by intentional binding of Co^{2+} to the CdS QD surfaces (dashed line).

nm. The right panel shows the visible absorption region. A broad and structured visible absorption feature with a maximum at 14430 cm^{-1} is observed that is associated with Co^{2+}. The dashed spectrum in Figure 1a shows the same sample after 23 h, and reveals a 50% loss of integrated intensity as well as a shift to lower average energy. The QD band gap absorption changes relatively little over the same time period.

Figure 1b shows the absorption spectrum of 0.9% Co^{2+}:CdS QDs (in pyridine) synthesized by the isocrystalline core/shell method described in Section II.A.ii. For these particles, a 3.0 nm diameter core was first synthesized exactly as in Figure 1a, around which a ca. 0.3 nm shell of CdS (approximately $^1/_2$ unit cell) was subsequently grown. An absorption feature centered at 13730 cm^{-1} is observed (right panel). A second feature, centered at ca. 6000 cm^{-1} and having roughly one-fifth the intensity, is also observed when deuterated pyridine was used as the solvent, but detailed analysis of this feature was precluded by the presence of overlapping vibrational overtones from solvent and/or residual surfactant (see Supporting Information, Figure S1). The left panel shows the CdS band gap absorption, the intensity of which has been scaled down by a factor of 1300 for presentation. This band gap transition is shifted to lower energy relative to that in Figure 1a, indicating particle growth to ca. 3.7 nm diameter. The dashed spectrum in Figure 1b was collected on the same sample 28 h after synthesis and shows no change.

Figure 2 shows visible absorption spectra of the sample described in Figure 1a collected at several times after initial particle synthesis. The first spectrum was collected ca. 2 h after initial coprecipitation. Subsequent spectra show decay of the absorption signal and a steady shift of intensity to lower energies with time. Figure 3 plots the 15220 cm^{-1} monochromatic absorption intensity taken from Figure 2 as a function of time. These data show that the absorption signal decay is biphasic. Biphasic kinetics are observed at all energies in Figure 2.

The solid line in Figure 4 shows the normalized visible absorption spectrum of 1.0% Co^{2+}:CdS QDs synthesized in the same way as those in Figure 1a, but capped with dodecanethiol and suspended in heptane. The Co^{2+} visible absorption bandwidth is similar to that in Figure 1a, but shows less resolved structure on the high-energy side. The dashed line in Figure 4 is the normalized absorption spectrum of surface-loaded Co^{2+}:CdS QDs suspended in pyridine, prepared by standard coprecipitation of CdS followed by addition of Co^{2+} ions to the inverted micelles just prior to capping. This spectrum is nearly identical with those in Figures 1a and 2 at short times, and also decays with time.

Figure 5a presents the visible absorption spectrum of 1.0% Co^{2+}:ZnS QDs (in pyridine) synthesized by the standard coprecipitation method following exactly the same procedure as used for Figure 1a. Figure 5b shows the absorption data for 1.0% Co^{2+}:ZnS QDs (in pyridine) synthesized by the isocrys-

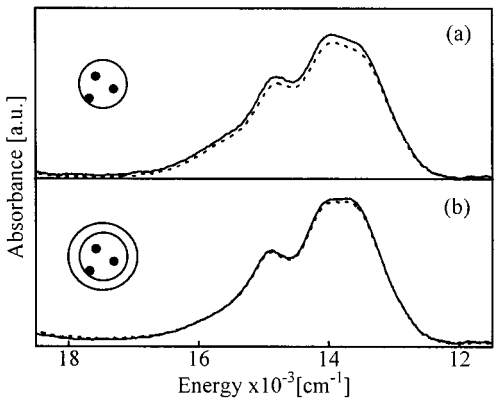

Figure 5. (a) Ligand-field absorption spectra (300 K) of 2.4 nm diameter 1.0% Co^{2+}:ZnS QDs in pyridine colloid solution. The solid line was collected 5 h and the dashed line 21 h after synthesis. (b) Ligand-field absorption spectra (300 K) of 2.9 nm diameter 1.0% Co^{2+}:ZnS QDs prepared by the isocrystalline core/shell method 5 (solid line) and 21 h (dashed line) after synthesis.

talline core/shell method exactly as used for Figure 1b. In contrast with the findings for Co^{2+}:CdS (Figure 1a,b), the absorption spectra of Co^{2+}:ZnS DMS-QDs prepared by these two methods (Figure 5a,b) are nearly identical. The dashed lines show the spectra of each sample after 21 h and reveal no changes in either case. These experiments were performed in pyridine for the purpose of comparison with those of Figure 1. Pyridine absorption occludes the ZnS QD band gap transitions, however, so these data could not be collected under the same conditions, and are therefore not shown. The ZnS QD band gap energies measured for solid films of the standard and core/shell particles were 38450 and 35700 cm^{-1}, respectively, indicating particle diameters of roughly 2.4 and 2.9 nm, respectively.

IV. Analysis and Discussion

A. Co^{2+} Spectroscopy. The electronic absorption spectroscopy of tetrahedral Co^{2+} ions has a rich history, and has played an important role in the development of ligand-field theory.[31] Tetrahedral and pseudo-tetrahedral Co^{2+} ions are well-known to exhibit intense visible absorption features that can serve as spectroscopic signals for investigating their electronic and geometric properties. The distinctive absorption signals of Co^{2+} have, for example, been employed to probe local environments of metalloprotein active sites in which Co^{2+} has been substituted for spectroscopically inactive ions (e.g. Zn^{2+}).[32,33]

Figure 6 shows an overview electronic energy level diagram appropriate for describing the ligand-field states of tetrahedral Co^{2+} (d^7) ions in the absence of spin−orbit coupling.[34] The vertical arrows indicate the three formally spin-allowed absorption transitions that have been observed in spectroscopic studies of bulk Co^{2+}-doped II−VI semiconductor single crystals at the ligand-field strength found for Co^{2+}:CdS ($10Dq/B \approx 4.75$).[35−38] To first order, spin−orbit coupling ($\zeta_{Co^{2+}\ \text{free ion}} = 515\ cm^{-1}$)

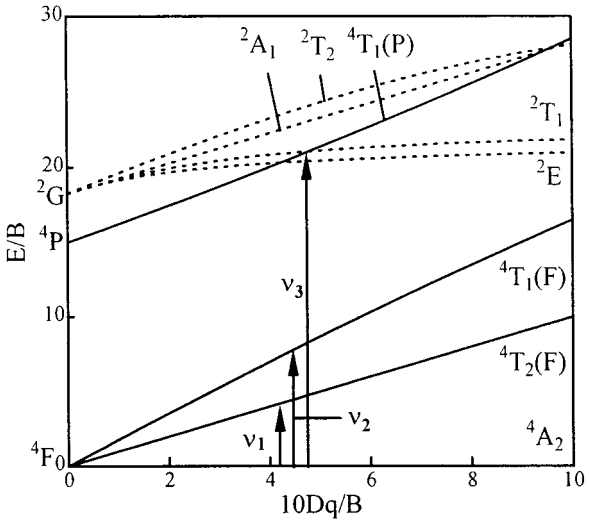

Figure 6. Ligand field energy level diagram for tetrahedral d^7 ions in the absence of spin−orbit coupling. The arrows indicate the three lowest energy spin-allowed transitions of Co^{2+} at the ligand field strength found for Co^{2+}:CdS. The arrows are labeled ν_1, ν_2, and ν_3 according to usage in the text.

splits each of the tetrahedral ^4T excited states into three spinor components. As seen from Figure 6, at the ligand field strength of CdS, the $^4T_1$(P) excited state is very close in energy to several doublet states derived from the ^2G free-ion term, and extensive spin−orbit mixing of quartet and doublet levels relaxes the spin-forbiddenness of transitions to these formally doublet excited states. Symmetry reduction may split these excited states further, and the effects of low-symmetry ligand fields have been systematically investigated by several authors.[31−33] Finally, vibronic mechanisms may make additional important contributions to the absorption band shapes. Because of the large number of overlapping absorption features in pseudo-tetrahedral Co^{2+} complexes, particularly in the $^4A_2 \rightarrow {}^4T_1$(P) region, the absorption bands associated with the three electronic transitions indicated in Figure 6 are often labeled $\nu_1(^4A_2 \rightarrow {}^4T_2)$, $\nu_2(^4A_2 \rightarrow {}^4T_1(F))$, and ν_3 ($^4A_2 \rightarrow {}^4T_1(P)$).[31] Our study focuses on the highest energy of these, the $\nu_3(^4A_2 \rightarrow {}^4T_1(P))$ band.

B. Standard Preparation of Co^{2+}-Doped CdS Quantum Dots. The absorption feature centered at 14600 cm^{-1} in Figure 1a is readily associated with the ν_3 ligand-field band characteristic of pseudo-tetrahedral Co^{2+}. This band is substantially broader and is shifted to higher average energies than the analogous band in bulk Co^{2+}:CdS.[35,36] These spectral differences are attributed to exposure of the majority of Co^{2+} ions to solvent in the Co^{2+}:CdS nanocrystals. This conclusion is confirmed by the data in Figure 4, which show that the ν_3 absorption band shape is influenced by changes in the identity of the capping ligand. Nanocrystals grown by standard coprecipitation and capped with dodecanethiol instead of pyridine (Figure 4, solid curve) yield a lower energy and less structured Co^{2+} ν_3 absorption band shape than those capped with pyridine (Figure 1a). The ligand-field absorption spectrum of thiol-capped Co^{2+}:CdS QDs approaches that of bulk Co^{2+}:CdS,[35,36] but still shows significant differences. This is consistent with the fact that the ligand field strength of an alkane thiol is similar to that of a lattice sulfide, but both are weaker field ligands than pyridine. The dashed line in Figure 4 provides further evidence that the spectra in Figure 1a are attributable to surface-bound Co^{2+}, showing that the intentional binding of Co^{2+} ions to the surfaces of undoped CdS nanocrystals yields a spectrum in pyridine that

(31) Lever, A. B. P. *Inorganic Electronic Spectroscopy*, 2nd ed.; Elsevier Science Publishers: Amsterdam, The Netherlands, 1984, and references therein.
(32) Bertini, I.; Luchinat, C. *Acc. Chem. Res.* **1983**, *16*, 272−279.
(33) Garmer, D. R.; Krauss, M. *J. Am. Chem. Soc.* **1993**, *115*, 10247−10257 and references therein.
(34) Tanabe, Y.; Sugano, S. *J. Phys. Soc. Jpn.* **1954**, *9*, 753−766.
(35) Weakliem, H. A. *J. Chem. Phys.* **1962**, *36*, 2117−2140.
(36) Pappalardo, R.; Dietz, R. E. *Phys. Rev.* **1961**, *123*, 1188−1203.
(37) Langer, J. M.; Baranowski, J. M. *Phys. Status Solidi B* **1971**, *44*, 155−166.
(38) Dreyhsig, J.; Litzenburger, B. *Phys. Rev. B* **1996**, *54*, 10516−10524.

is nearly identical with the one observed at short times in Figure 1a. These results indicate that a large fraction of the Co^{2+} ions reside on CdS nanocrystal surfaces when Co^{2+}:CdS QDs are prepared by the standard coprecipitation method.

In addition to having a broader band shape, the sample from Figure 1a is found to be unstable over time when suspended in pyridine solution (Figure 1a, dashed). After 23 h, the integrated Co^{2+} visible absorption intensity is reduced to ca. 50% of its original value, and after 750 h less than 20% of the original intensity remains (Figure 2). Concomitant with the loss in integrated intensity is a shift of this absorption feature to lower energies, shown in Figure 2. This instability is attributed to solvation of surface-bound Co^{2+} ions by pyridine. In pyridine, Co^{2+} exists as $Co(py)_6^{2+}$, which shows a visible absorption maximum at 20400 cm^{-1} having a molar extinction coefficient 1 to 2 orders of magnitude smaller than those of tetrahedrally coordinated Co^{2+},[31] and is therefore not observed on the same intensity scale. Monitoring the absorption decay kinetics of Figure 2 quantitatively reveals that Co^{2+} solvation is biphasic (Figure 3), and these data are fit by a double-exponential function to yield $k_1 = 0.48\ h^{-1}$ ($\pm 0.02\ h^{-1}$) and $k_2 = 0.017\ h^{-1}$ ($\pm 0.002\ h^{-1}$). The values of k_1 and k_2 are independent of the energy monitored, but the ratio of magnitudes of the fast vs slow components is largest for data measured at highest energies (16 at 16 700 cm^{-1} vs 1 at 13 200 cm^{-1}). These observations implicate the presence of two transient species involved in the solvation process.

The large difference between rate constants k_1 and k_2 allows the absorption spectra of these two transient chromophores to be deconvoluted and compared with the spectrum of internally doped Co^{2+}:CdS. Figure 7a compares the normalized visible absorption spectra of (i) internally doped Co^{2+}:CdS QDs from Figure 1b synthesized by the isocrystalline core/shell method (see Section IV.C), (ii) the slow-decaying component from Figure 1a (given as the difference spectrum 84−750 h), and (iii) the fast-decaying component (given as the difference spectrum 2.0−2.8 h). These three spectra are good representations of the three dominant forms of Co^{2+} observed. Although spectra i, ii, and iii may involve some minor convolution of signals, or even minor intensities from additional species, further manipulation of the data is not warranted.

A brief discussion of the band shapes observed in Figure 7a is necessary, as it relates to our analysis and conclusions. Close inspection reveals that the distinct peaks observed in spectra i, ii, and iii are irregularly spaced in each case. Spectrum i, which reproduces that of bulk Co^{2+}:CdS at 300 K (see Section IV.C), shows three major peaks at 13 330, 13 700, and 14 510 cm^{-1}. The absorption band sharpens upon cooling to 15 K, and two maxima are observed at 13 600 and 14 490 cm^{-1}, with several shoulders (see Supporting Information, Figure S2). This 15 K spectrum is similar to, but not as well resolved as, the spectra reported for bulk Co^{2+}:CdS single crystals at 4.2 K, where the structure has been attributed primarily to spin−orbit splitting within the $^4T_1(P)$ term and inter-term spin−orbit mixing of these levels with nearby doublet levels.[35,36] The spacing we observe between the two major peaks is 890 cm^{-1}. This spacing is far greater than the highest energy lattice phonon energies of nanocrystalline CdS (ca. 300 cm^{-1}),[39] and implicates important electronic contributions to this structure. We note that although the highest energy vibrations are only ca. 300 cm^{-1} in the ground state, substantially greater vibrational energy spacings may exist in the excited states due to the nuclear-coordinate dependence

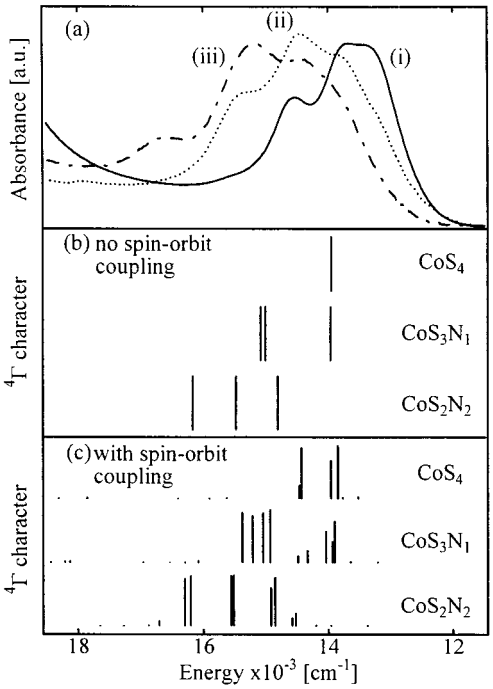

Figure 7. (a) Normalized 300K absorption spectra of Co^{2+} in CdS QDs: (i) internal Co^{2+} from Figure 1b, (ii) slow-decay species from Figure 1a, represented by the difference spectrum (84−750 h), and (iii) fast-decay species from Figure 1a, represented by the difference spectrum (2.0−2.8 h). (b) Calculated energies of Co^{2+} quartet excited states in the ν_3 region for $Co(\mu_4\text{-}S)_4$, $Co(\mu_4\text{-}S)_3(N(py))_1$, and $Co(\mu_4\text{-}S)_2(N(py))_2$ obtained by neglecting spin−orbit coupling. (c) Calculated energies and relative quartet ($^4\Gamma$) character of Co^{2+} excited states in the ν_3 region for $Co(\mu_4\text{-}S)_4$, $Co(\mu_4\text{-}S)_3(N(py))_1$, and $Co(\mu_4\text{-}S)_2(N(py))_2$ obtained by inclusion of spin−orbit coupling. Parameters: $e_\sigma(S) = 2365\ cm^{-1}$, $e_\pi(S) = 0\ cm^{-1}$, $e_\sigma(N(py)) = 3860\ cm^{-1}$, $e_{\pi\perp}(N(py)) = 110\ cm^{-1}$ (anisotropic). Spin−orbit coupling, $\zeta = 500\ cm^{-1}$. B values for $Co(\mu_4\text{−}S)_x(N(py))_{4-x}$ were estimated as the weighted average between $B = 665\ cm^{-1}$ for $Co(\mu_4\text{−}S)_4$ and $B = 690\ cm^{-1}$ for $Co(N(py))_4$, and $C/B = 4.75$.

of the inter-term spin−orbit mixing, which can lead to strongly perturbed and anharmonic excited-state potential energy surfaces.[40] Modification of Figure 6 to include spin−orbit coupling reveals several strong coupling interactions in the Franck−Condon region that should contribute to the ν_3 spectra of Co^{2+}:CdS (see Supporting Information, Figure S3).[35] Such vibronic effects are not accounted for by purely electronic ligand field theory models such as those applied in refs 35 and 36, and that applied below.

At 300 K, irregular peak spacings of ca. 670 and 880 cm^{-1} are observed in spectrum ii of Figure 7a. Since this spectrum is obtained by temporal deconvolution, the corresponding 15 K spectrum could not be cleanly measured. The 15 K spectrum of a sample prepared as in Figure 1a and measured after ca. 50 h shows maxima at 13 910, 14 510, and 15 440 cm^{-1} that are clearly attributable to spectrum ii, yielding energy spacings of 600 and 930 cm^{-1} (see Supporting Information, Figure S2). Similarly, spectrum iii in Figure 7a shows irregular spacings of 750 to 1435 cm^{-1} at 300 K. No 15 K absorption data were collected for this transient species. Because of the irregular spacings observed, the structure in spectra ii and iii is not solely vibronic, but likely involves important contributions from low-symmetry and spin−orbit coupling effects as well. Despite this complexity, to a very good approximation all of the ν_3 intensity

(39) See for example: Balandin, A.; Wang, K. L.; Kouklin, N.; Bandyopadhyay, S. *Appl. Phys. Lett.* **2000**, *76*, 137−139.

(40) Bussiere, G.; Reber, C. *J. Am. Chem. Soc.* **1998**, *120*, 6306−6315.

in each of these three spectra ultimately derives from the allowedness of the $^4A_2 \rightarrow {}^4T_1(P)$ parent transition, and previous studies have shown that the center of gravity of the ν_3 band accurately reflects the average ligand field strength experienced by the central Co^{2+} ion.[31,41] For the purposes of characterization, the energetic shifts between the centers of gravity of spectra i, ii, and iii in Figure 7a are therefore more informative than the changes in band shape. The experimental centers of gravity determined from Figure 7a are approximately (i) 13 730, (ii) 14 460, and (iii) 15 180 cm^{-1}.

To describe the spectra of Figure 7a in more detail, ligand field calculations have been performed within the framework of the angular-overlap model (AOM).[41,42] The ligand-field parameters for Co^{2+}:CdS QDs are estimated from the literature values for bulk Co^{2+}:CdS (Dq = 315 cm^{-1}, B = 665 cm^{-1}, $C/B = 4.75$, ζ = 500 cm^{-1}).[35,36] For the purpose of converting these values to AOM parameters we note that the valence orbitals of the lattice sulfides are sp^3 hybridized due to tetrahedral coordination by four cations. The lattice sulfides are therefore involved exclusively in σ-bonding interactions with the Co^{2+}. To emphasize this fact when discussing localized Co^{2+} ligand-field environments, we hereafter refer to the lattice sulfides by use of the coordination chemistry notation, μ_4-S. The above ligand field parameters and the theoretical AOM relationship for tetrahedral ligand field strengths provided in eq 1[41,42] thus yield $e_\sigma(S) = 2365$ cm^{-1} and $e_\pi(S) = 0$ cm^{-1}.

$$|10Dq(T_d)| = \frac{4}{9}(3e_\sigma - 4e_\pi) \qquad (1)$$

Pyridine AOM parameters of $e_\sigma(N(py)) = 3860$ cm^{-1} and $e_{\pi\perp}(N(py)) = 110$ cm^{-1} (anisotropic) were estimated from literature values[41] for $Co(py)_6^{2+}$ and eq 1. Using these values with no iterative fitting, the transition energies anticipated for all four pseudo-tetrahedral $Co(\mu_4\text{-}S)_{4-x}(N(py))_x$ species ($0 \le x \le 4$) were calculated with and without inclusion of spin−orbit coupling. The results for $x = 0$, 1, and 2 are shown as the vertical bars in Figure 7b,c.

Figure 7b shows the excited-state energies calculated for the parent spin-allowed ν_3 transitions in the absence of spin−orbit coupling. As observed previously,[31,41] the $^4T_1(P)$ excited state in tetrahedral symmetry is rather insensitive to the reduction in symmetry caused by ligand substitution, showing only relatively small (<1400 cm^{-1}) electronic splittings. Figure 7b shows that these quartet excited states shift to higher average energy upon substitution of lattice sulfides by pyridine nitrogens in the Co^{2+} coordination sphere, due to the stronger ligand field strength of the latter. The centers of gravity of the calculated electronic levels for the three species shown in Figure 7b in the absence of spin−orbit coupling are 13 950, 14 685, 15 475 cm^{-1}, reproducing the experimental average energies in Figure 7a very well.[43] Other possible structures including $Co(\mu_4\text{-}S)_1(N(py))_3$ and $Co(\mu_4\text{-}S)_3(N(py))_2$ have been considered and yield calculated energies that are inconsistent with the experimental data.

Figure 7c shows the transitions calculated upon inclusion of spin−orbit coupling. Spin−orbit coupling broadens the calculated ν_3 bands and gives them complex structure by splitting the quartet states and mixing these levels with nearby doublets. Estimating electronic absorption intensities as proportional to the quartet character of each excited state, the bar graphs of Figure 7c show the intensity distributions anticipated in the absence of vibronic coupling.[44] As with Figure 7b, the calculated energies reproduce the experimental trends well; the centers of gravity of Figure 7b are generally preserved, but the intensity distributions are irregularly broadened upon inclusion of spin−orbit coupling. In comparing these calculated results to the experimental data of Figure 7a, it is noted that the experimental data involve additional vibronic band shape contributions arising from differences between the ground- and excited-state potential surfaces as described above. These contributions include low-temperature Franck−Condon profiles and temperature-dependent vibrational hot bands. The ν_3 band of spectrum i, centered at 13 730 cm^{-1} in Figure 7a, is narrower and centered at ca. 13 980 cm^{-1} at 15 K, for example (see Supporting Information, Figure S1). Because of the complexity of these absorption bands, no iterative refinement of the literature ligand-field parameters was attempted.

In summary, electronic structure calculations with literature ligand-field parameters predict ν_3 energies and shifts for the tetrasulfido and mono- and di-pyridyl-substituted Co^{2+} ions that are very similar to those observed experimentally in spectra i, ii, and iii of Figure 7a, respectively. These results allow the conclusion that Co^{2+} ions in CdS QDs prepared by simple coprecipitation and suspended in pyridine (Figure 1a) initially exist predominantly as surface-bound $Co(\mu_4\text{-}S)_2(N(py))_2$, having an average ν_3 energy of $E_{avg} \approx 15180$ cm^{-1} and a solvation rate constant of $k_1 = 0.48$ h^{-1}. A significant amount of $Co(\mu_4\text{-}S)_3(N(py))_1$ ($E_{avg} \approx 14460$ cm^{-1}, $k_2 = 0.017$ h^{-1}) is also initially present on the surface, but relatively little (<20%) Co^{2+} is actually incorporated within the QDs. This analysis is summarized in Scheme 1, which shows surface-bound Co^{2+} ions undergoing successive coordination by pyridine and eventual solvation.[45] In 3.0 nm diameter nanocrystals only ca. 35% of the cation substitution sites are anticipated to be at the surface. Our results therefore indicate that precipitation of CdS in the presence of Co^{2+} ions leads to a nonstatistical distribution of Co^{2+} within the CdS nanocrystals.

Scheme 1

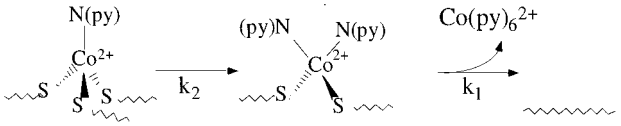

C. Isocrystalline Core/Shell Synthesis of Co^{2+}-Doped CdS Quantum Dots. We have used the information gained from the above electronic absorption experiments to refine our DMS-QD synthetic methodology, and report here a core/shell method that allows convenient synthesis of internally doped Co^{2+}:CdS QDs. Core/shell methods have received wide attention in the quantum dot literature because of the importance of controlling surface properties of nanocrystals, where surfaces account for a large percentage of the total material.[1,2,46−48] The term core/shell is generally used to describe a composite material in which

(41) Figgis, B. N.; Hitchman, M. A. *Ligand Field Theory and its Applications*; Wiley: New York, 2000, and references therein.

(42) Gerloch, M.; Slade, R. C. *Ligand-Field Parameters*; Cambridge University Press: Cambridge, UK, 1973, and references therein.

(43) In the tetrahedral weak-field limit, $E(^4T_1(P)) \approx 12Dq + 15B$. With use of this relationship and weighted average values for Dq and B, the calculated ν_3 centers of gravity are 13755, 14385, and 15023 cm^{-1} for x = 0, 1, and 2, respectively, also in agreement with the assignments of (i), (ii), and (iii).

(44) Note that the graphical intensity representation in Figure 7c may be misleading in instances involving near degeneracy of levels, and is primarily intended to illustrate energy splittings.

(45) Fitting the data of Figure 3 using coupled linear rate equations as implied by Scheme 1 yields pseudo-first-order rate constants indistinguishable from those presented phenomenologically in Figure 3. Similarly, taking the kinetics to begin upon pyridine solvation and not upon particle formation also does not alter k_1 and k_2 significantly.

(46) Hines, M. A.; Guyot-Sionnest, P. *J. Phys. Chem.* **1996**, *100*, 468−471.

Scheme 2

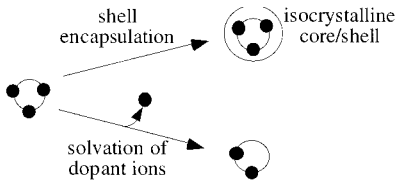

a layer (the shell) of one semiconductor or insulator is epitaxially grown around a nucleus (the core) of another. In the present study, the core consists of the Co^{2+}:CdS DMS-QD synthesized by standard coprecipitation in inverted micelles, while the shell consists of the pure semiconductor CdS. To differentiate these core/shell materials from the usual heterocrystalline core/shell materials, we refer to them as isocrystalline core/shell particles.

The absorption spectrum of Co^{2+}:CdS QDs prepared by the isocrystalline core/shell method is shown in Figure 1b. This spectrum is very similar to that of bulk Co^{2+}:CdS,[35,36] confirming that Co^{2+} ions substitute for lattice Cd^{2+} ions and have a tetrasulfido coordination environment in this isocrystalline core/shell preparation. When deuterated pyridine is used, a 6000 cm^{-1} absorption band is also observed, but is partially obscured by vibrational overtone absorption (see Supporting Information, Figure S1). This low-energy band is assigned as the $^4A_2 \rightarrow {}^4T_1(F)$ ligand-field transition of the same tetrahedral Co^{2+}, again consistent with reported bulk Co^{2+}:CdS spectra. Importantly, time-dependent absorption measurements show that the isocrystalline core/shell Co^{2+}:CdS particles are stable in pyridine solution, yielding no loss of Co^{2+} over an extended time scale (Figure 1b, dashed). These data indicate that the previously surface-bound dopant ions are encapsulated by growth of a layer of CdS around the Co^{2+}:CdS DMS-QD core. This is illustrated in Scheme 2, where the large circles represent boundaries of CdS particles and the black dots represent Co^{2+} ions. The isocrystalline core/shell method thus provides a rapid and convenient solution to the problem of surface-bound dopant ions widely encountered in DMS-QD preparations.

D. Co^{2+}-Doped ZnS Quantum Dots. To address the origin of the nonstatistical dopant distribution found in Co^{2+}:CdS QDs formed by standard coprecipitation, we have prepared Co^{2+}-doped ZnS QDs by the same two methods as used in Figure 1. In contrast with the results obtained for Co^{2+}:CdS QDs, the visible absorption spectrum of Co^{2+}:ZnS QDs prepared by the standard coprecipitation method and suspended in pyridine (Figure 5a) does not show a substantially broadened band shape, but closely resembles that of bulk Co^{2+}:ZnS.[35] The spectrum of the sample obtained by the isocrystalline core/shell method (Figure 5b) is similar but somewhat better resolved. Both samples are stable against Co^{2+} solvation in pyridine (Figure 5, dashed lines). From these data, we conclude that Co^{2+} ions are readily incorporated into the ZnS lattice during ZnS nanocrystal growth. We note that even in the limit of isotropic substitution, the particles formed by standard coprecipitation are expected to show greater Co^{2+} inhomogeneity than those formed by the isocrystalline core/shell method due to the large number of surface substitution sites available.

These results demonstrate that transition-metal doping of CdS and ZnS nanocrystals by standard coprecipitation methods differs substantially. Although Co^{2+} doping of ZnS nanocrystals is approximately statistical, Co^{2+} doping of CdS nanocrystals is distinctly nonstatistical. We conclude that the large mismatch in ionic radii of Co^{2+} (0.74 Å) and Cd^{2+} (0.97 Å) is responsible for Co^{2+} exclusion during CdS nanocrystal growth, with Co^{2+} binding to the surface only after growth is complete. In contrast, the similarity of Zn^{2+} (0.74 Å) and Co^{2+} ionic radii allows isotropic incorporation of Co^{2+} into ZnS QDs during nanocrystal growth. These results reflect the importance of ionic radius mismatches in determining the internal energies, and hence stabilities with respect to dissociation, of doped nanocrystals.[49] As shown in Scheme 2, subsequent growth of a CdS shell around Co^{2+}:CdS QDs prepared by standard coprecipitation entraps the surface-bound Co^{2+} ions, producing a stable bulklike dopant environment.

E. Relationship to Mn^{2+}-Doped DMS-QDs. Our observations with Co^{2+}:CdS and Co^{2+}:ZnS QDs lend some insight into the reported properties of Mn^{2+}-doped II−VI QDs, which have received tremendous attention recently. Recent studies have shown that coprecipitation methods for preparing Mn^{2+}:CdS and Mn^{2+}:CdSe QDs also result in poor internal incorporation of dopant ions.[4,19] In the study of Mn^{2+}:CdSe QDs,[4] thorough washing with pyridine led to loss of all Mn^{2+} EPR signal intensity, and it was concluded that Mn^{2+} resided primarily at the particle surfaces. To overcome the problem of Mn^{2+} incorporation into CdSe lattices, a methodology involving organometallic precursors such as $Mn_2(\mu\text{-SeMe})_2(CO)_8$ rather than simple Mn^{2+} salts was developed, and its success demonstrated.[4] Other authors have recently questioned the correctness of these findings, however, as they have demonstrated that high-quality Mn^{2+}:ZnSe QDs can be made by direct coprecipitation without the use of organometallic precursors.[5] Our results suggest that these two sets of experimental observations can be reconciled by recognizing that the difference between Mn^{2+} doping of CdSe (or CdS) and ZnSe (or ZnS) likely arises from the more favorable match between Zn^{2+} (0.74 Å) and Mn^{2+} (0.80 Å) ionic radii than that between Cd^{2+} (0.97 Å) and Mn^{2+}, as observed for Co^{2+}. Furthermore, the data in Figure 1b show that internally doped DMS-QDs involving such large lattice mismatches can also be prepared without the use of organometallic precursors, by employing an isocrystalline core/shell method. This synthetic methodology is generally applicable, and should provide a simple alternative route for the synthesis of other DMS-QDs involving lattice mismatches.

Aging of Mn^{2+}-doped CdS QDs for ca. 48 h prior to capping has also been shown to yield higher quality internally doped Mn^{2+}:CdS samples.[26,27] Although aging led to loss of ca. 40% of the Mn^{2+} ions in these preparations, the final product showed resolved manganese hyperfine EPR splittings and enhanced emission intensities, indicating better incorporation of the remaining dopant ions into the CdS lattice.[27] We have verified that this conclusion also applies to Co^{2+}:CdS QDs by using absorption spectroscopy to follow Co^{2+}:CdS QD aging in inverted micelle solutions under our standard synthesis conditions (data not shown). With aging, we observe particle growth by the Ostwald ripening mechanism, a decrease in Co^{2+} absorption intensity by ca. 60%, and a concomitant change of the ν_3 absorption signal from that of Figure 1a (solid) to one that is similar to that of Figure 1b. The aging layer formed over a period of many hours or days is thus analogous to the isocrystalline shell introduced in the core/shell method over a period of minutes. The latter technique requires substantially less time, is more easily controlled to yield the desired particle size, and retains a greater percentage of dopant ions, ensuring their localization within the QD lattice.

(47) Dabbousi, B. O.; Rodriguez-Viejo, J.; Mikulec, F. V.; Heine, J. R.; Mattoussi, H.; Ober, R.; Jensen, K. F.; Bawendi, M. G. *J. Phys. Chem. B* **1997**, *101*, 9463−9475.

(48) Talapin, D. V.; Rogach, A. L.; Kornowski, A.; Haase, M.; Weller, H. *Nano Lett.* **2001**, *1*, 207−211.

(49) Ahmadi, T. S.; El-Sayed, M. A. *J. Phys. Chem. A* **1997**, *101*, 690−693.

V. Conclusion

Using ligand-field electronic absorption spectroscopy as a probe, we have found that simple coprecipitation methods for preparing Co^{2+}:CdS QDs yield predominantly surface-bound dopant ions, and have attributed this to a large mismatch between the cationic radii of Co^{2+} and Cd^{2+}. To overcome this problem, an isocrystalline core/shell synthetic methodology has been developed that allows convenient preparation of high-quality internally doped DMS-QDs suitable for further optical study, even in cases involving dissimilar dopant and host cations. In a broader context, this study demonstrates the utility of electronic absorption spectroscopy as a quantitative probe of dopant ion geometries, electronic structure, and phase separation dynamics in DMS-QDs.

Acknowledgment. The authors thank the University of Washington and its Center for Nanotechnology for supporting this research. P.V.R. thanks the University of Washington Center for Nanotechnology for his Graduate Research Award.

Supporting Information Available: Figures showing (S1) the 300 K VIS/NIR absorption spectrum of 0.9% Co^{2+}:CdS prepared by the isocrystalline core/shell method and suspended in deuterated pyridine, compared with that of bulk Co^{2+}:CdS[35] (S2) comparison of the 15 K visible absorption spectrum of 0.9% Co^{2+}:CdS QDs prepared by the isocrystalline core/shell method with that of 2.3% Co^{2+}:CdS QDs prepared by the standard method and measured ca. 50 h after synthesis, and (S3) a d^7 electronic energy level diagram showing the effects of spin−orbit coupling in the region describing visible absorption of Co^{2+}:CdS (PDF). This material is available free of charge via the Internet at http://pubs.acs.org.

JA0115215